Co-design of Regular Layout and Mooring Systems for Floating Offshore Wind Farms on Complex Seabed

Zehai Huang[1], Boan Lu[1], Renshen Tan[2], Xinwei Shen[1*]
[1] *Tsinghua Shenzhen International Graduate School, Tsinghua University, Shenzhen, China*
[2] *Guangdong Electric Power Design Institute, Guangzhou, China*

***Abstract*—Floating offshore wind farms (FOWFs) are becoming increasingly vital in the global transition to renewable energy, especially in deep-water regions. This paper presents a co-design approach for the regular layout and mooring systems of FOWFs on complex seabed. We first construct a Mixed-Integer Linear Programming (MILP) grid-based model to determine the initial positions of floating wind turbines (FWTs) using a seabed depth proxy. Using this as the initial solution, a continuous optimization model is formulated to adjust FWTs coordinates and mooring lines (MLs) angles, while precisely solving for the optimal MLs lengths to maximize the profit of the FOWFs. Case studies demonstrate the effectiveness of the proposed method in enhancing the economic performance of the FOWFs.**

Index Terms-- offshore wind farm; layout optimization; mooring lines optimization; complex seabed

NOMENCLATUREN

Acronyms

FOWFs	Floating offshore wind farms
FWTs	Floating wind turbines
MLs	Mooring lines
MILP	Mixed-integer Linear programming
GWO	Grey wolf optimization

Indexes and Sets

$\xi \in \Xi$	Index and set of the wind scenarios
$m, n \in M$	Index and set of FWTs positions
$k, s \in K$	Index and set of FWTs MLs number
$i, j \in I$	Index and set of candidate FWTs grids
$r \in C_{\text{row}}$	Index and set of rows in FOWFs
$c_r \in C_{r,\text{col}}$	Index and set of columns in FOWFs in row r
$t \in T$	Index and set of FOWFs operating times
$p \in \mathcal{P}$	Index and set of layout patterns in FOWFs
$g \in G$	Index and set of active rows in FOWFs
$u \in U_g$	Index and set of the number of FWTs in the row where the g-th FWT is located

Parameters

V_i/V_j	Wind speed at FWT i / j
$V_{\text{in}}/V_{\text{out}}$	Cut-in/ Cut-out speed
V_{rated}	Rated speed
V_∞^ξ	Free-stream wind speed at wind scenario ξ
P_∞^ξ	FWTs output power in wind scenario ξ without wake effects
$P_{i,j}^\xi$	The power due to wake effects from FWT i on FWT j at wind scenario ξ
C_{T}	Thrust coefficient
R_0	WTs radius
W_{ij}	Wake deficit caused by WT j to WT i
P_{rated}	Rated power of WT
Q^{FWT}	FWTs number
E_{elec}	Electricity price
α	Wake decay constant
β	Power constant
π^ξ	Occurrence probability of wind scenario ξ
θ^{ML}	ML declination angle
ω	Discounted rate
η	FOWFs power reduction coefficient
$capex_{\text{base}}$	FWTs platform base cost
$capex_{\text{ML}}$	FWTs ML cost
$capex_{\text{A}}$	FWTs anchor cost
f^{plat}	FWTs platform cost growth coefficient
f^{elec}	FOWFs electrical system cost ratio coefficient
f_0	FOWFs O&M basic cost ratio coefficient
f_{add}	FOWFs O&M cost growth coefficient

Variables

x_i	Binary variables for FWTs installation of the i-th grid
P_j^ξ	Output power of FWT j at wind scenario ξ
θ_m	The angle of the ML of the m-th FWT
$\phi_{m,k}$	Angle of the k-th ML of the m-th FWT
(z_{1m}, z_{2m})	Coordinates of the m-th FWTs
$\boldsymbol{z}_m/\boldsymbol{z}_n$	Coordinate vector of the m-th/ n-th FWTs
$\boldsymbol{z}_{g,u}$	The position vector of the u-th FWT in g row
$\mathbf{a}_{m,k}$	Anchor coordinate vector of the k-th ML of m-th FWT

This work was supported in part by National Natural Science Foundation of China (52477102), GuangDong Basic and Applied Basic Research Foundation of China (2023A1515240055), as well as the Excellent Youth Basic Research Fund of Shenzhen (RCYX20231211090430053) (*Corresponding author: Xinwei Shen*).

979-8-3315-8138-1

$\mathbf{w}_{m,k}$	The vector of the k-th ML of m-th FWT
$l_{m,k}^{\text{sea}}$	Projection of the k-th ML of the m-th FWT on the sea surface
$h(\mathbf{a}_{m,k})$	Depth at the anchor location of the k-th ML of the m-th FWT
$l_{m,k}^{\text{ML}}$	Length of the k-th ML of the m-th FWT
$\delta_{r,p}$	Binary variables for the p-th layout pattern in the r-th row
y_p	Binary variables for the p-th layout pattern

I. INTRODUCTION

Offshore wind energy has become a key component of the global transition to renewable energy. With the rapid development of offshore wind power, the scale of its deployment is continuously expanding. Offshore wind energy development is gradually moving from nearshore to deeper offshore regions. By the end of 2024, the global installed capacity of offshore wind power had reached approximately 83 gigawatts (GW), enough to power 73 million households [1].

Wake effects can lead to a reduction in the power generation of wind farms by 10% to 20% [2]. For nearshore fixed-bottom wind farms, the layout design mainly focuses on the positioning of the turbines. However, for floating offshore wind farms (FOWFs), the layout must also take into account the design of the mooring lines (MLs), which is influenced by the complex seabed conditions. In practical engineering applications, OWFs are typically constructed in a regular layout [3], which facilitates O&M [4] and reduces infrastructure construction costs [5].

Numerous studies have been conducted on the optimization of OWF layouts without constraints of regular layout [6]- [11]. Among these, [6]-[7] developed Mixed-Integer Linear Programming (MILP) models, while [8] established a Mixed-Integer Quadratic Programming (MIQP) model. All of these studies employed a grid-based approach, where the wind farm area is divided into grids, with the grid centers serving as potential candidate sites for turbine installation. However, the majority of studies employ heuristic algorithms for optimizing OWFs layouts, such as algorithms (GA) [9], particle swarm optimization (PSO) [10], and differential evolution algorithms (DEA) [11]. Some researchers, considering the practical engineering requirements, have incorporated regular layouts into the optimization of offshore wind farm layouts. References [4] and [12] parameterized the regular layout by defining variables such as the number of rows and columns, the row-column angles, and the distance between WTs in rows and columns. In [13], WTs are arranged uniformly along the cross-wind direction, while in the main wind direction, WTs are deployed with staggered spacing.

Currently, research on the optimization of FOWF layouts and mooring systems is limited [14]-[15]. Reference [14] accounts for a buffer zone in the MLs of FWTs but neglects the impact of water depth on ML length. Reference [15] considers both seabed conditions and water depth effects on MLs and anchors. However, the inclusion of water depth increases computational complexity, resulting in slower optimization, limiting the study to only six FWTs. Furthermore, none of these studies addresses the incorporation of regular layouts, which present challenges for practical implementation.

In this paper, we propose a co-design approach for optimizing the regular layout and MLs of FOWFs in complex seabed conditions. Leveraging a ML proxy and regular-layout constraints, we first formulate a MILP grid model to obtain initial FWT positions. We then apply grey wolf optimization (GWO) [16] to refine FWT coordinates and seabed-informed ML placement. A real-world case study in Hainan, China, shows that the method materially improves the FOWF's lifetime net present value (NPV).

II. MODELING OF FLOATING OFFSHORE WIND FARMS

A. Wake Model

This paper adopts the 2D wake model proposed by Tian et al [17]. In a FOWF, the wind speed at a downstream FWT j under the wake influence of an upstream FWT i is:

$$V_j = V_i\left(1 - W_{ij}\right) \tag{1}$$

where W_{ij} represents the wake-induced loss factor, and is given by:

$$W_{ij} = \frac{\left(1-\sqrt{1-C_{\mathrm{T}}}\right)R_0^2}{{R_1}^2}\left(1-\cos\left(\frac{\pi}{R_1}\cdot R^{\text{radial}}+\pi\right)\right) \tag{2}$$

where R^{radial} is the radial distance from the center of the wake region, and R_1 is the wake radius at a downstream distance from upstream FWT, which can be calculated by:

$$R_1 = R_0 + \alpha R^{\text{radial}} \tag{3}$$

B. Power Output Model

In FOWFs, the power curve of a FWT can be approximated as follows:

$$P(V) = \begin{cases} 0 & 0 \le V \le V_{\text{in}} \\ \beta V^3 & V_{\text{in}} \le V \le V_{\text{rated}} \\ P_{\text{rated}} & V_{\text{rated}} \le V \le V_{\text{out}} \\ 0 & V \ge V_{\text{out}} \end{cases} \tag{4}$$

Accounting for multi-wake superposition within the FOWFs, the power of a downstream FWT can be computed as:

$$P_j^{\xi} = P_{\infty}^{\xi} - \sum_i x_i\left(P_{\infty}^{\xi} - P_{i,j}^{\xi}\right) \quad \forall i,j,\xi \tag{5}$$

where $P_{i,j}^{\xi}$ is computed as follows:

$$P_{i,j}^{\xi} = \beta[V_{\infty}^{\xi}(1 - W_{i,j}^{\xi})]^3 \quad \forall i,j,\xi \tag{6}$$

C. Modeling of MLs

In practice, several ML configurations are used for FWT station-keeping, e.g., three-line, four-line, and six-line systems. This paper focuses on the three-line (3-ML) configuration, which is shown in Fig.1. Let the FWT position be $\boldsymbol{z}_m = (z_{1m}, z_{2m})$ and the fairlead depth be h^{deep}. The MLs are attached to the fairlead and deployed toward the seabed with a

979-8-3315-8138-1

declination angle θ^{ML} relative to the horizontal. For a 3-ML system, the azimuths are uniformly spaced by 120°:

$$\phi_{m,k} = \theta_m + \{0^{\circ}, 120^{\circ}, 240^{\circ}\} \quad \forall m, k \tag{7}$$

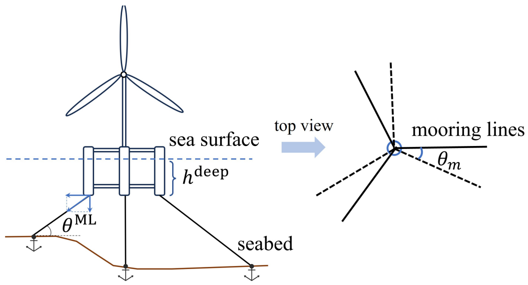

Figure 1. Schematic of a FWT and its MLs

Denote by $l_{m,k}^{\mathrm{sea}}$ the horizontal projection of the k-th ML and by $\mathbf{a}_k$ its anchor on the seabed. The anchor coordinates follow the planar geometry:

$$\mathbf{a}_{m,k} = \mathbf{z}_m + l_{m,k}^{\mathrm{sea}} \begin{bmatrix} \cos\phi_{i,k} \\ \sin\phi_{i,k} \end{bmatrix} \quad \forall m, k \tag{8}$$

Let $h(\mathbf{a}_k)$ be the local water depth at the anchor location. With the specified declination angle, the fairlead–seabed relation is:

$$h^{\mathrm{deep}} + l_{m,k}^{\mathrm{sea}} tan\theta^{\mathrm{ML}} = h(\mathbf{a}_{m,k}) \ \forall m, k \tag{9}$$

The ML length is then calculated by:

$$l_{m,k}^{\mathrm{ML}} = \sqrt{{l_{m,k}^{\mathrm{sea}}}^2 + \left(h(\mathbf{a}_{m,k}) - h^{\mathrm{deep}}\right)^2} \ \forall m, k \tag{10}$$

III. Methodology

This paper co-designs the regular layout and MLs of FOWFs on complex seabed. In this study, "complex seabed" specifically refers to seabed terrain characterized by significant variations in water depth. Firstly, a grid-based MILP model is formulated to determine FWT locations under regular-layout constraints. Based on the model's discrete nature, ML lengths are approximated via a depth-based proxy evaluated at each FWT position, and the initial FWT coordinates are obtained with a commercial solver. Using this as the initial solution, we then build a continuous-coordinate model and apply GWO to fine-tune FWT positions and optimize their MLs to maximize the FOWF's NPV.

A. MILP Model based on ML Proxy Function

To obtain a high-quality initial solution, we formulate a MILP with the following objective:

$$max \ \ NPV(x_i) = Profit - \sum_{i \in I} x_i \left(C^{\mathrm{WT}} + C_i^{\mathrm{plat}} + C_i^{\mathrm{ML}} + C_i^{\mathrm{elec}} + C_i^{\mathrm{O\&M}}\right) \tag{11}$$

where $Profit$ is discounted revenue of FOWFs, C^{WT} is per-FWT CAPEX, while C_i^{plat}, C_i^{ML}, C_i^{elec}, and $C_i^{\mathrm{O\&M}}$ are site-specific platform, ML, electrical, and O&M present costs, respectively. The site-specific costs are linear functions of the depth d_i and are computed as:

$$Profit = E_{\mathrm{elec}} \cdot \sum_{t \in T} \frac{\sum_{\xi \in \Xi} \sum_{i \in I} \pi^{\xi} \cdot P_i^{\xi}}{(1+\omega)^t} \cdot \eta \ \ \forall i, \xi \tag{12}$$

$$C_i^{\mathrm{plat}} = capex_{\mathrm{base}} + f^{\mathrm{plat}} \cdot d_i \ \ \forall i \tag{13}$$

$$C_i^{\mathrm{ML}} = capex_{\mathrm{ML}} \cdot \sum_{k \in K} l_{i,k}^{\mathrm{ML}} + |K| \cdot capex_{\mathrm{A}} \ \ \forall i \tag{14}$$

$$C_i^{\mathrm{elec}} = f^{\mathrm{elec}} \cdot \left(C^{\mathrm{WT}} + C_i^{\mathrm{plat}} + C_i^{\mathrm{ML}}\right) \ \forall i \tag{15}$$

$$C_i^{\mathrm{O\&M}} = \sum_{t \in T} \frac{f_i^{\mathrm{O\&M}}\left(C^{\mathrm{WT}} + C_i^{\mathrm{plat}} + C_i^{\mathrm{ML}} + C_i^{\mathrm{elec}}\right)}{(1+\omega)^t} \ \ \forall i \tag{16}$$

$$f_i^{\mathrm{O\&M}} = f_0 + f_{\mathrm{add}} \cdot d_i \ \ \forall i \tag{17}$$

In the MILP, the ML angles are fixed at 0°, and the ML length $l_{i,k}^{\mathrm{ML}}$ in (14) is approximated by using the local water depth at the corresponding FWT site as a proxy for the anchor depth.

This paper adopts a pattern-based layout approach, first defining the set of layout patterns $\mathcal{P} = \{(c_0^{(t)}, e_p) | c_0^{(t)} \in C_{\mathrm{col}}, e_p \geq 10R_0, (\boldsymbol{t}_{r,p} - 1)\, e_p \leq |C_{r,\mathrm{col}}| - 1,\ e_t \in \mathbb{Z}_+, \boldsymbol{t}_p \in \mathbb{Z}_+\}$, where $c_0^{(t)}$ is starting column, e_t is an integer grid spacing, and $\boldsymbol{t}_{r,p}$ represents the number of selected grids in row r for pattern p. Specifically, suppose a pattern p starts from the initial column $c_0^{(t)}$, and then selects a position every e_p columns, continuing until the selected columns exceed the total column limit $|C_{r,\mathrm{col}}|$, as shown in Fig.2. To ensure FWT MLs stay within the FOWFs, their lengths are pre-calculated based on depth and compared with the minimum distance to the FOWFs boundary. If ML exceeds this distance, the site is invalid for FWT placement.

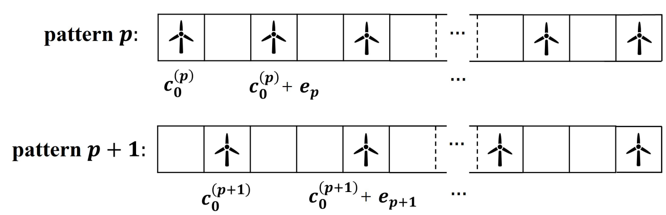

Figure 2. The layout patterns for FWTs per row

The constraints of the MILP model are as follows:

$$\sum_i x_i = Q^{\mathrm{FWT}} \quad \forall i \tag{18}$$

$$\sum_p y_p = 1 \tag{19}$$

$$\delta_{r,p} \leq y_p \tag{20}$$

$$\sum_p \delta_{r,p} \leq 1 \tag{21}$$

$$x_{\mathbb{N}_r} = \sum_p \varepsilon_{r,p}\, \delta_{r,p} \tag{22}$$

979-8-3315-8138-1

$$x_i + x_j \le 1 \quad \forall i,j : distance_{i,j} < 10R_0 \tag{23}$$

$$0 \le P_i^{\xi} \le P_i^{\text{rated}} x_i \qquad \forall i, \xi \tag{24}$$

$$x_i, x_j, y_p, \delta_{r,p}, \varepsilon_{r,p} \in \{0,1\} \quad \forall i,j,r,p \tag{25}$$

Equation (18) represents the wind turbine count constraint for the wind farm. The regular layout constraints are expressed by Equations (19)–(22), where only one layout pattern can be selected per row. Specifically, $\varepsilon_{(r,p)} = \{0,1\}_p^{\mathbb{N}_r}$ is the binary vector for pattern p in row r. Equation (23) enforces the minimum safety distance constraint, requiring a separation of at least $10R_0$ between FWTs. Equations (5)-(6) and (24) define the power constraints for FOWFs.

B. Continuous Model with Accurate ML Computation

To ensure that the continuous model generates high-quality feasible solutions, the solution from the MILP model is used as the feasible starting point. In the continuous model solved by GWO, the ML for each FWT is precisely computed based on the turbine position and ML angle. The complete model is outlined as follows:

$$max \;\; NPV\left(\boldsymbol{z}_{g,1}, d, \theta_m\right) \tag{26}$$

$$\boldsymbol{z}_{g,1} \in A\left(x_g\right) \;\; \forall g \tag{27}$$

$$\boldsymbol{z}_{g,u} = \boldsymbol{z}_{g,1} + (u-1)d \cdot \boldsymbol{e} \;\; \forall m, u \tag{28}$$

$$||\boldsymbol{z}_m - \boldsymbol{z}_n||_2 \ge 10R_0 \;\; \forall m, n \tag{29}$$

$$\inf_{u,v \in [0,1]} ||\mathbf{w}_{m,k}(u) - \mathbf{w}_{n,s}(v)||_2 \ge l^{\text{safe}} \;\; \forall m \ne n, k, s \tag{30}$$

The objective function (26) also aims to maximize the NPV of the FOWFs. Equation (27) ensures that the first turbine in each row can only move within its designated grid range. Equation (28) dictates that the positions of the remaining turbines in the row are determined by the first turbine, with adjacent turbines having the same vertical coordinate and a horizontal distance of d, where $\boldsymbol{e}$ is the direction vector. Equations (29)–(30) impose minimum safety distance constraints between FWTs, and between MLs. In accordance with ISO 19901-7, MLs and anchors must be at least 100 m apart from other offshore installations, so the safety distance l^{safe} for MLs is set to 100m.

IV. Case Study

A. Case Conditions

The proposed co-design method for the regular layout and MLs will be validated on a FOWF in Hainan, China. The wind farm consists of 30 WT263-13MW turbines, with ML angles set to 0°. The depth ranges from 320 to 480 meters, and the initial layout of the wind farm is shown in Fig. 3. The average annual wind speed of the wind farm is 8.83 m/s. The specific wind distribution is obtained from the Global Wind Atlas [18], and for the sake of brevity, it is not replotted here. The FWT parameters are shown in Table I, and the economic parameters of FOWFs (including mooring-related costs which reference [14]) are provided in Table II. The GWO settings include a wolf pack size of 60 and 600 iterations. The simulations were performed using MATLAB 2022b and Gurobi 10 on a system featuring an Intel Core i7-1360P CPU, 16 GB of RAM, and an Intel Iris Xe integrated GPU.

B. Result Analyses

Since the predominant wind directions are at 40°, 60°, and 180°, the primary wind direction is taken as the average of these three angles, which is 80°. The FOWFs is arranged perpendicular to the 80° direction. The optimized layout

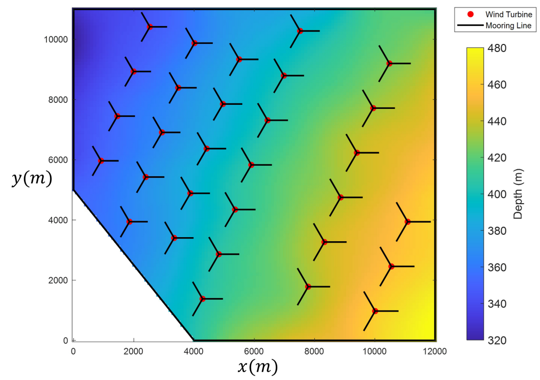

Figure 3. The initial layout of Hainan FOWF

TABLE I. FWTs Parameters

FWTs number	30	Wake expansion coefficient	0.05
FWTs diameter	263m	Thrust coefficient	0.88
Rated power	13MW	Power reduction coefficient	85%
Rated speed	10.6m/s	ML number	3
Cut-in speed	3m/s	Fairlead depth	20m
Cut-out speed	25m/s	ML declination angle	30°

TABLE II. FOWFs Economic Parameters

T	20years	$capex_{\text{ML}}$	1,188¥/m
ω	5%	$capex_{\text{A}}$	2.9×10⁶¥/anchor
E_{elec}	0.42¥/kWh	f^{elec}	12%
C_{WT}	4.5×10⁷¥/FWT	f_0	1.5%
$capex_{\text{base}}$	6×10⁷¥/platform	f_{add}	0.005%/m
f^{plat}	50,000¥/m		

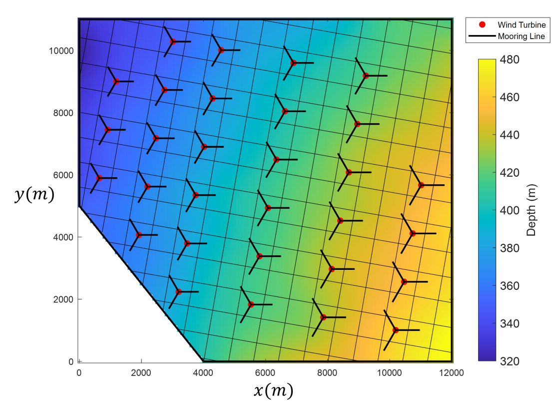

Figure 4. The optimized layout obtained by the MILP model

TABLE III. COMPARISON OF ECONOMIC PERFORMANCE AND POWER PRODUCTION

	NPV	**Net power**	**Profit**	**FWT cost**	**Platform cost**	**MLs cost**	**Electrical cost**	**O&M cost**
Initial layout	1.82×10^9¥	1.77×10^5kW	7.38×10^9¥	1.35×10^9¥	2.33×10^9¥	2.84×10^8¥	4.76×10^8¥	1.12×10^9¥
MILP model	1.98×10^9¥	1.80×10^5kW	7.51×10^9¥	1.35×10^9¥	2.32×10^9¥	2.86×10^8¥	4.75×10^8¥	1.09×10^9¥
Continuous model	2.48×10^9¥	1.85×10^5kW	7.72×10^9¥	1.35×10^9¥	2.23×10^9¥	2.81×10^8¥	4.64×10^8¥	9.15×10^9¥

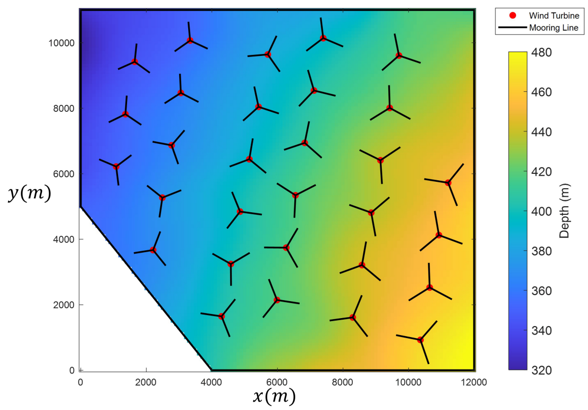

Figure 5. The optimized layout obtained by the continuous model

obtained by the MILP model is shown in Fig. 4. Using this layout as the initial solution for the continuous model, the GWO algorithm is used to further fine-tune the FWTs' coordinates, turbine spacing, and the ML angles for each turbine. The ML costs are then calculated, resulting in the final layout shown in Fig. 5.

The comparison of economic performance and power production is shown in TABLE III. Compared to the initial layout with a wake loss of 10.65%, the MILP model first identifies a high-quality discrete solution that reduces wake loss by 1.61%. Subsequently, the continuous model further refines these positions, ultimately achieving a total wake loss reduction of 4.16%. Moreover, the costs associated with MLs and depth in the final layout are significantly reduced, resulting in an NPV of ¥2.48 billion, which is an additional profit of ¥0.66 billion compared to the initial layout. This clearly demonstrates that the co-design approach proposed in this paper effectively enhances the economic benefits of wind farms.

V. CONCLUSION

In this paper, we propose a co-design approach for regular layout and MLs. Specifically, we first develop a grid-based MILP model, with an objective function that includes the proxy costs associated with the MLs. A micro-siting method based on layout patterns is proposed to achieve a regular layout. Next, a continuous coordinate model is established, where FWT coordinates are adjusted, the distance between FWTs and ML angles are optimized based on the initial solution of the MILP model, allowing for precise calculation of ML lengths. A case study of a FOWF in Hainan, China, demonstrates that the proposed method can increase turbine power output while effectively reducing costs related to MLs and water depth, ultimately enhancing the economic benefits of the FOWF.

Future work will include a comprehensive O&M cost model and account for the impact of different geotechnical conditions to achieve a more precise characterization of costs.

REFERENCES

[1] Global Wind Energy Council (GWEC), “Global Offshore Wind Report 2025”, GWEC, Brussels, Belgium, 2025.

[2] R. J. Barthelmie et al., “Modelling and measuring flow and wind turbine wakes in large wind farms offshore,” *Wind Energy*, vol. 12, no. 5, pp. 431–444, Jul. 2009.

[3] S. Astariz and G. Iglesias, “Enhancing Wave Energy Competitiveness through Co-Located Wind and Wave Energy Farms. A Review on the Shadow Effect,” *Energies*, vol. 8, no. 7, pp. 7344–7366, Jul. 2015.

[4] S. González, Á. L. T. García, M. B. Payán, J. R. Santos, and Á. G. G. Rodríguez, “Optimal wind-turbine micro-siting of offshore wind farms: A grid-like layout approach,” *Appl. Energy*, vol. 200, pp. 28-38, 2017.

[5] A. Neubert, A. Shah, and W. Schlez, “MAXIMUM YIELD FROM SYMMETRICAL WIND FARM LAYOUTS,” *Proceedings of DEWEK*, vol. 98, 2010.

[6] P. Fagerfjäll, “Optimizing wind farm layout: more bang for the buck using mixed integer linear programming,” *Chalmers University of Technology and Gothenburg University,* vol. 111, 2010.

[7] J.-A. Pérez-Rúa, M. Stolpe, and N. A. Cutululis, “A neighborhood search integer programming approach for wind farm layout optimization,” *Wind Energy Sci.*, vol. 8, no. 9, pp. 1453–1473, Sep. 2023.

[8] S. D. O. Turner, D. A. Romero, P. Y. Zhang, C. H. Amon, and T. C. Y. Chan, “A new mathematical programming approach to optimize wind farm layouts,” *Renew. Energy*, vol. 63, pp. 674–680, Mar. 2014.

[9] J. S. González, M. B. Payán, and J. R. Santos, “A new and efficient method for optimal design of large offshore wind power plants,” *IEEE Trans. Power Syst.*, vol. 28, no. 3, pp. 3075–3084, Aug. 2013.

[10] S. Paul and Z. H. Rather, “A pragmatic approach for selecting a suitable wind turbine for a wind farm considering different metrics,” *IEEE Trans. Sustain. Energy*, vol. 9, no. 4, pp. 1648–1658, Oct. 2018.

[11] Y. Wang, H. Liu, H. Long, Z. Zhang, and S. Yang, “Differential Evolution With a New Encoding Mechanism for Optimizing Wind Farm Layout,” *IEEE Trans. Ind. Inform.*, vol. 14, no. 3, pp. 1040–1054, Mar. 2018.

[12] A. P. J. Stanley and A. Ning, “Massive simplification of the wind farm layout optimization problem,” *Wind Energy Sci.*, vol. 4, no. 4, pp. 663–676, Dec. 2019.

[13] G. Gualtieri, “A novel method for wind farm layout optimization based on wind turbine selection,” *Energy Convers. Manage.*, vol. 193, pp. 106–123, Aug. 2019.

[14] M. Hall, M. Biglu, S. Housner, K. Coughlan, M. Y. Mahfouz, and E. Lozon, “Floating Wind Farm Layout Optimization Considering Moorings and Seabed Variations,” *J. Phys.: Conf. Ser.*, vol. 2767, no. 6, p. 062038, Jun. 2024.

[15] H. Sun, M. Li, T. Fan, and C. Cai, “Investigation of Floating Offshore Wind Farm Layout Optimization Considering Mooring Line Constraints,” *JMSE*, vol. 13, no. 1, p. 54, Dec. 2024.

[16] S. Mirjalili, S. M. Mirjalili, and A. Lewis, “Grey Wolf Optimizer,” Advances in Engineering Software, vol. 69, pp. 46–61, Mar. 2014.

[17] L. Tian, W. Zhu, W. Shen, N. Zhao, and Z. Shen, “Development and validation of a new two-dimensional wake model for wind turbine wakes,” *J. Wind Eng. Ind. Aerodyn.*, vol. 137, pp. 90–99, Feb. 2015.

[18] N. N. Davis et al., “The Global Wind Atlas: A high-resolution dataset of climatologies and associated web-based application,” Bull. Amer. Meteorological Soc., vol. 104, no. 8, pp. E1507–E1525, 2023.

979-8-3315-8138-1